Photo-acoustic sub-micrometer modifications of glass by pair of femtosecond laser pulses

Yoshio Hayasaki,[1,*] Mitsuhiro Isaka,[1] Akihiro Takita,[1] Satoshi Hasegawa,[1] and Saulius Juodkazis[2,3]

[1]*Center for Optical Research and Education (CORE), Utsunomiya University, 7-1-2 Yoto, Utsunomiya 321-8585, Japan*
[2]*Centre for Micro-Photonics, Faculty of Engineering and Industrial Sciences, Swinburne University of Technology, Hawthorn, VIC 3122, Australia*
[3]*Melbourne Centre for Nanofabrication, 151 Wellington Road, Clayton, VIC 3168, Australia*
[*]*hayasaki@opt.utsunomiya-u.ac.jp*

Abstract: We present time-resolved studies of glass densification created by an acoustic phenomenon: collision of the transverse and longitudinal sound waves inside glass. Localization of the permanent denisfied region has a lateral cross section ~ 0.4 μm and is approximately half of the wavelength of femtosecond laser pulses which were used to generate breakdown and launched shock waves inside glass. Controlled time delay between two closely spaced irradiation spots reveals dynamics and relaxation (electronic, thermal, stress) of glass after excitation. The observed phenomenon is important for femtosecond direct laser writing and recording of waveguide couplers using multiple beams.

© 2012 Optical Society of America

OCIS codes: (140.3390) Laser materials processing; (350.3850) Materials processing; (160.1245) Artificially engineered materials.

References and links

1. Z. Yu, A. Raman, and S. Fan, "Fundamental limit of nanophotonic light trapping in solar cells," Proc. Natl. Acad. Sci. USA **107**, 17491–17496 (2010).
2. H. K. Wickramasinghe, R. C. Bray, V. Jipson, C. F. Quate, and J. R. Salcedo, "Photoacoustics on a microscopic scale," Appl. Phys. Lett. **33**, 923–926 (1978).
3. C. R. Otey, W. T. Lau, and S. Fan, "Thermal rectification through vacuum," Phys. Rev. Lett. **104**, 154301 (2010).
4. J. Morikawa, E. Hayakawa, T. Hashimoto, R. Buividas, and S. Juodkazis, "Thermal imaging of a heat transport in regions structured by femtosecond laser," Opt. Express **19**, 20542–20550 (2011).
5. S. Danworaphong, T. A. Kelf, O. Matsuda, M. Tomoda, Y. Tanaka, N. Nishiguchi, O. B. Wright, Y. Nishijima, K. Ueno, S. Juodkazis, and H. Misawa, "Real-time imaging of acoustic rectification," Appl. Phys. Lett. **99**, 201910 (2011).
6. E. Vanagas, J. Kawai, D. Tuzilin, I. Kudryashov, A. Mizuyama, K. G. Nakamura, K. Kondo, S. Koshihara, M. Takesada, K. Matsuda, S. Juodkazis, V. Jarutis, S. Matsuo, and H. Misawa, "Glass cutting by femtosecond pulsed irradiation," J. Microlith. Microfab. Microsyst. **3**, 358–363 (2004).
7. A. Schubnel, S. Nielsen, J. Taddeucci, S. Vinciguerra, and S. Rao, "Photo-acoustic study of subshear and supershear ruptures in the laboratory," Earth Planet. Sci. Lett. **308**, 424–432 (2011).
8. E. Gamaly, A. Vailionis, V. Mizeikis, W. Yange, A. Rode, and S. Juodkazis, "Warm dense matter at the bench-top: fs-laser induced confined microexplosion," High Energy Density Phys. **8**, 13–17 (2012).
9. A. Vailionis, E. G. Gamaly, V. Mizeikis, W. Yang, A. Rode, and S. Juodkazis, "Evidence of super-dense Aluminum synthesized by ultra-fast micro-explosion," Nat. Commun. **2**, 445 (2011).
10. A. Vogel, S. Busch, and U. Parlitz, "Shock wave emission and cavitation bubble generation by picosecond and nanosecond optical breakdown in water," J. Acoust. Soc. Am. **100**, 148–165 (1996).

#164236 - $15.00 USD Received 29 Mar 2012; revised 11 Apr 2012; accepted 17 Apr 2012; published 27 Apr 2012

11. A. Vogel and V. Venugopalan, "Mechanisms of pulsed laser ablation of biological tissues," Chem. Rev. **103**, 577–644 (2003).
12. M. Ams, G. D. Marshall, P. Dekker, J. A. Piper, and M. J. Withford, "Ultrafast laser written active devices," Laser Photon. Rev. **3**, 535–544 (2009).
13. L. Shah, A. Arai, S. Eaton, and P. Herman, "Waveguide writing in fused silica with a femtosecond fiber laser at 522 nm and 1 MHz repetition rate," Opt. Express **13**, 1999–2006 (2005).
14. J. Siebenmorgen, T. Calmano, K. Petermann, and G. Huber, "Highly efficient Yb:YAG channel waveguide laser written with a femtosecond-laser," Opt. Express **18**, 16035–16041 (2010).
15. S. Nolte, M. Will, J. Burghoff, and A. Tünnermann, "Femtosecond waveguide writing: a new avenue to three-dimensional integrated optics," Appl. Phys. A **77**, 109–111 (2003).
16. G. Cerullo, R. Osellame, S. Taccheo, M. Marangoni, D. Polli, R. Ramponi, P. Laporta, and S. D. Silvestri, "Femtosecond micromachining of symmetric waveguides at 1.5μm by astigmatic beam focusing," Opt. Lett. **27**, 1938–1940 (2002).
17. B. Poumellec, L. Sudrie, M. Franco, B. Prade, and A. Mysyrowicz, "Femtosecond laser irradiation stress induced in pure silica," Opt. Express **11**, 1070–1079 (2003).
18. J. Canning, M. Lancry, K. Cook, A. Weickman, F. Brisset, and B. Poumellec, "Anatomy of a femtosecond laser processed silica waveguide," Opt. Mater. Express **1**, 998–1008 (2011).
19. G. Cheng, K. Mishchik, C. Mauclair, E. Audouard, and R. Stoian, "Ultrafast laser photoinscription of polarization sensitive devices in bulk silica glass," Opt. Express **17**, 9515–9525 (2009).
20. Y. Bellouard and M.-O. Hongler, "Femtosecond-laser generation of self-organized bubble patterns in fused silica," Opt. Express **19**, 6807–6821 (2011).
21. Y. Bellouard, M. Dugan, A. A. Said, and P. Bado, "Thermal conductivity contrast measurement of fused silica exposed to low-energy femtosecond laser pulses," Appl. Phys. Lett. **89**, 161911 (2006).
22. M. Sakakura, T. Tochio, M. Eida, Y. Shimotsuma, S. Kanehira, M. Nishi, K. Miura, and K. Hirao, "Observation of laser-induced stress waves and mechanism of structural changes inside rock-salt crystals," Opt. Express **19**, 17780–17789 (2011).
23. M. Sakakura, M. Terazima, Y. Shimotsuma, K. Miura, and K. Hirao, "Thermal and shock induced modification inside a silica glass by focused femtosecond laser pulse," J. Appl. Phys. **109**, 023503 (2011).
24. K. K. Seet, S. Juodkazis, V. Jarutis, and H. Misawa, "Feature-size reduction of photopolymerized structures by femtosecond optical curing of SU-8," Appl. Phys. Lett. **89**, 024106 (2006).
25. E. Vanagas, I. Kudryashov, D. Tuzhilin, S. Juodkazis, S. Matsuo, and H. Misawa, "Surface nanostructuring of borosilicate glass by femtosecond nJ energy pulses," Appl. Phys. Lett. **82**, 2901–2903 (2003).
26. V. V. Temnov, K. S.-Tinten, P. Zhou, and D. von der Linde, "Ultrafast imaging interferometry at femtosecond-laser-excited surfaces," J. Opt. Soc. Am. B **23**, 1954–1964 (2006).
27. P. Stampfli and K. H. Bennemann, "Time dependence of the laser-induced femtosecond lattice instability of Si and GaAs: role of longitudinal optical distortions," Phys. Rev. B **49**, 7299–7305 (1994).
28. Y. Hayasaki, M. Isaka, A. Takita, and S. Juodkazis, "Time-resolved interferometry of femtosecond-laserinduced processes under tight focusing and close-to optical breakdown inside borosilicate glass," Opt. Express **19**, 5725–5734 (2011).
29. Y. Hayasaki, K. Iwata, S. Hasegawa, A. Takita, and S. Juodkazis, "Time-resolved axial-view of the dielectric breakdown under tight focusing in glass," Opt. Mater. Express **1**, 1399–1408 (2011).
30. F. Quéré, S. Guizard, and P. Martin, "Time-resolved study of laser-induced breakdown in dielectrics," Europhys. Lett. **56**, 138–144 (2001).
31. M. Lancry, N. Groothoff, B. Poumellec, S. Guizard, N. Fedorov, and J. Canning, "Time-resolved plasma measurements in Ge-doped silica exposed to infrared femtosecond laser," Phys. Rev. B **84**, 245103 (2011).
32. D. G. Papazoglou and S. Tzortzakis, "Physical mechanisms of fused silica restructuring and densification after femtosecond laser excitation," Opt. Mater. Express **1**, 625–632 (2011).
33. D. G. Papazoglou and S. Tzortzakis, "In-line holography for the characterization of ultrafast laser filamentation in transparent media," Appl. Phys. Lett. **93**, 041120 (2008).
34. A. Marcinkevicius, V. Mizeikis, S. Juodkazis, S. Matsuo, and H. Misawa, "Effect of refractive index-mismatch on laser microfabrication in silica glass," Appl. Phys. A **76**, 257–260 (2003).
35. E. Gaižauskas, E. Vanagas, V. Jarutis, S. Juodkazis, V. Mizeikis, and H. Misawa, "Discrete damage traces from filamentation of Bessel-Gauss pulses," Opt. Lett. **31**, 80–82 (2006).
36. T. Hashimoto, S. Juodkazis, and H. Misawa, "Void formation in glass," New. J. Phys. **9**, 253 (2007).
37. C.-S. Zha, R. J. Hemley, H.-K. Mao, T. S. Duffy, and C. Meade, "Acoustic velocities and refractive index of SiO_2 glass to 57.5 GPa by Brillouin scattering," Phys. Rev. B **50**, 13105–13112 (1994).
38. E. Gamaly, S. Juodkazis, V. Mizeikis, H. Misawa, A. Rode, and W. Krolokowski, "Modification of refractive index by a single fs-pulse confined inside a bulk of a photo-refractive crystal," Phys. Rev. B **81**, 054113 (2010).
39. A. A. Ionin, S. I. Kudryashov, S. V. Makarov, L. V. Seleznev, and D. V. Sinitsyn, "Generation and detection of superstrong shock waves during ablation of an aluminum surface by intense femtosecond laser pulses," JETP Lett. **94**, 35–39 (2011).
40. M. Watanabe, S. Juodkazis, H.-B. Sun, S. Matsuo, and H. Misawa, "Luminescence and defect formation by

#164236 - $15.00 USD Received 29 Mar 2012; revised 11 Apr 2012; accepted 17 Apr 2012; published 27 Apr 2012
(C) 2012 OSA

visible and near-infrared irradiation of vitreous silica," Phys. Rev. B **60**, 9959–9964 (1999).
41. J. Morikawa, A. Orie, T. Hashimoto, and S. Juodkazis, "Thermal and optical properties of the femtosecond-laser-structured and stress-induced birefringent regions of sapphire," Opt. Express **18**, 8300–8310 (2010).
42. E. Brasselet and S. Juodkazis, "Intangible pointlike tracers for liquid-crystal-based microsensors," Phys. Rev. A **82**, 063832 (2010).
43. S. Juodkazis, V. Mizeikis, and H. Misawa, "Three-dimensional microfabrication of materials by femtosecond lasers for photonics applications," J. Appl. Phys. **106**, 051101 (2009).
44. S. Matsuo, S. Juodkazis, and H. Misawa, "Femtosecond laser microfabrication of periodic structures using a microlens array," Appl. Phys. A **80**, 683–685 (2004).
45. L. Bressel, D. de Ligny, C. Sonneville, V. Martinez-Andrieux, V. Mizeikis, R. Buividas, and S. Juodkazis, "Femtosecond laser induced density changes in GeO_2 and SiO_2 glasses: fictive temperature effect," Opt. Mater. Express **1**, 605–613 (2011).

1. Introduction

Acoustic and thermal phenomena occurring on the scales from sub-micrometer to tens of micrometers is an active research field spanning nano-/micro-mechanics, fluidics, light trapping [1], thermal transport and heat management [2]. For example, a thermal diode function [3–5] can be realized on nano-to-micro-scale useful for applications in thermal energy harvesting by thermo-electrical materials to power NEMS/MEMS devices. Modifications of materials by acoustic and shock waves have been reported on surfaces, where tensile stresses generated by shock reflection caused spallation [6]. Photo-acoustic methods are also relevant for an in-lab modeling of large scale phenomena such as earthquakes [7] and formation of high-pressure/density phases [8, 9]. For thermal and acoustic research on micro- and nano-scale, ultra-short laser pulses are useful tools to generate instantaneous heating and build up thermo-elastic stresses applicable in cell surgery and generation of coherent phonons in solid state materials [10, 11]. Optical modification of materials by fs-laser pulses is already a well established field of optical memory and waveguide engineering [12–18], while, acoustical and thermal effects triggered by fs-laser pulses are active field of fundamental research [19–24] important to practical applications in laser micro-fabrication, scribing and surface nano-structuring [25, 26]. Since fs-laser pulses creates an "instantaneous" pressure source upon thermalization, the acoustic frequency range of excitation is very broad up to GHz [5]. Strong optical excitation are shown to lead to lattice instability on sub-1 ps times [27].

Recently, we have demonstrated development of an interferometric pump-probe time-resolved imaging technique capable to characterize modifications in glass induced by fs-laser pulses [28, 29] in both *lateral* and *axial* cross sections at the conditions of dielectric breakdown with sub-wavelength resolution. Pump-probe techniques are required to resolve ultra-fast phenomena related to free carrier generation and self-trapping [30, 31], lattice instability in crystalls [27] which lead to formation of amorphous regions, stress, and defects [17, 18, 32, 33]. Since the pressure from a point-like pressure source is decaying along its propagation as $P \propto r^{-3}$, where r is the radius, a high spatial resolution is required to monitor transient shock and pressure patterns generated by ultra-short tightly focused laser pulses.

Here we demonstrate a time-resolved lateral transient of the dielectric breakdown when two closely spaced pump pulses are tightly focused inside glass. The amplitude and phase changes of interferograms obtained by a Michelson interferometer reveals densification of glass on the line connecting the two irradiation spots. Transient and permanent densification of glass are created away from the irradiation location and can be accounted for by acoustical interaction of intense transverse and longitudinal sound waves. Temporal and spatial analysis reveals that such modifications can strongly alter direct laser writing of waveguide couplers when laser spots are scanned in close proximity.

#164236 - $15.00 USD Received 29 Mar 2012; revised 11 Apr 2012; accepted 17 Apr 2012; published 27 Apr 2012
(C) 2012 OSA

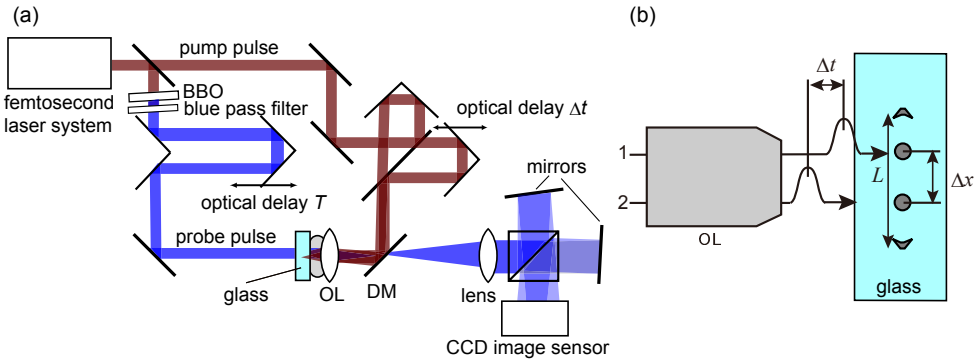

Fig. 1. (a) Interferometric pump-probe imaging. (b) Schematics of two pump pulses (1,2) delayed in time by Δt and separated in space by Δx. The side-spots depict location of glass densification induced by shock wave; separation between them is L.

2. Experimental

The pump-probe (800 nm - 400 nm) fs-laser setup for single-pulse measurements is described in our recent work [28]. Differently from that geometry, here, we split the pump pulse in two with possibility of a fine tuning separation, Δx, between them (Fig. 1(b)).

The interferometric detection and numerical procedures to obtain time - resolved phase and amplitude maps of fs-pulse interaction with glass are described in previous work [28]. The resolution limit of the optical imaging part was 0.4 μm for the probe pulse $\lambda_{pr} = 0.4$ μm using an objective lens of numerical aperture $NA = 1.25$. The resolution limit of the image processing was $r_{ip} = 1/h = 0.22$ μm defined by the cutoff frequency h of the Hann window and the magnification of the microscope [28].

The focal spot was located approximately 10 μm below surface inside a borosilicate glass (D263, Schott) plate; the values of relevant parameters are: $\rho = 2.51$ g/cm^3 at 20°C - the mass density, $Y = 72.9$ kN/mm^2 - the Young modulus, $\sigma = 0.208$ - the Poisson ratio, and with bulk modulus $B = 41.6$ kN/mm^2 given by $Y = 3B(1-2\sigma)$. The longitudinal sound speed was directly measured by phase imaging in a single pulse experiment [28] and was $v_l = 5.44 \pm 0.12$ km/s.

Location of the geometrical focus has been determined at low pulse energies when small positive phase changes were induced and spherical aberration was negligible [34] since the immersion oil is matching the refractive index of glass, $n_{800} \approx n_{400} \simeq 1.52$ at 800 and 400 nm wavelengths, respectively. The waist at the focus is estimated as $\omega = 0.61\lambda/NA \simeq 0.39$ μm which is a radius of the Airy disk pattern. The depth of focus - the double Rayleigh length $2z_R = 2\frac{\pi\omega^2}{\lambda} n_{800} \simeq 1.8$ μm (at FWHM), where $\lambda = 0.8$ μm is the central wavelength of the laser pump pulse in air.

Pump pulse energy, E_p, is given at the focus; the transmission of the objective lens was directly measured. The threshold of self-focusing in borosilicate glass is ~ 1.8 MW. It is defined by the nonlinear refractive index and is similar in various multi-component glasses [35, 36], where it is approximately twice lower than in pure silica. The side imaging was carried out with 400 nm probe collected with the same $NA = 1.25$ objective lens. Hence, the smallest recognizable features were on the order of ~ 0.4 μm. Experiments were carried out at a narrow window of pump pulse energies $E_p = 30 - 60$ nJ when a shock wave induced densification was observed outside the irradiated region. Pulse duration at the focus was optimized by pre-chirping

#164236 - $15.00 USD Received 29 Mar 2012; revised 11 Apr 2012; accepted 17 Apr 2012; published 27 Apr 2012
(C) 2012 OSA

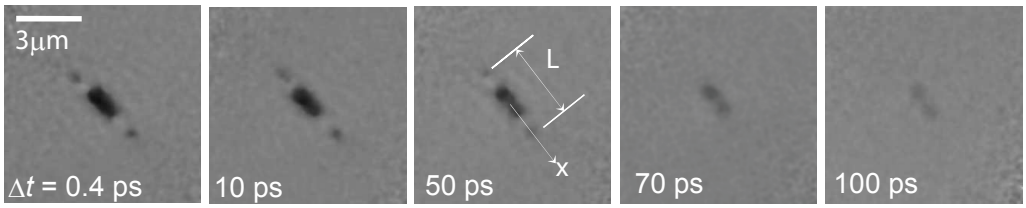

Fig. 2. Acoustically-induced densification (the darker side spots) at the end of relaxation $T = \infty$. Lateral phase images around the focus region of two-pulse irradiation after the end of relaxation; the darker regions are more dense. Time separation, Δt, between two pump pulses at 800 nm wavelength is shown; phase scale is from $-\pi$ to π. Spatial separation between two pump pulses of energy $E_1 = E_2 = 50$ nJ was $\Delta x = 1.0$ μm (measured experimentally); L is the length between the densified side spots; polarization of pulses was linear (horizontal in the image plane). The upper irradiation site is where the first pulse arrived (darker appearance), the lower site is location of the second (delayed) pulse.

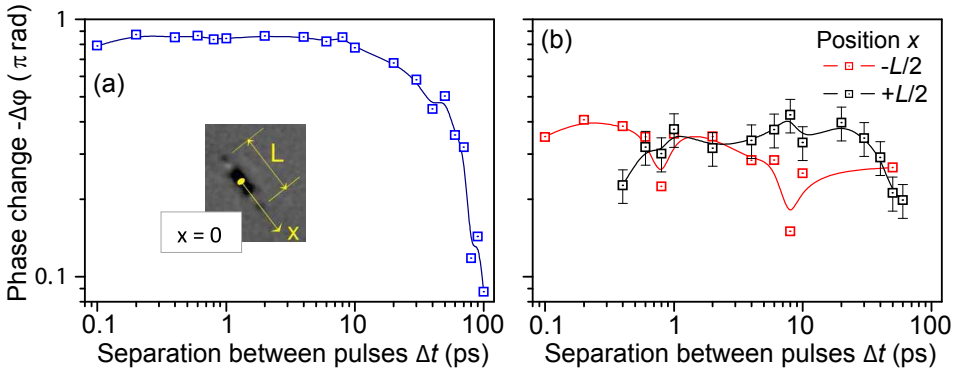

Fig. 3. Phase at the location the middle point between the two pump pulses $x = 0$ (a) and at the "side spots" (b) vs separation between pulses, Δt, when $\Delta x = 1$ μm. $E_1 = E_2 =$ 50 nJ. Lines are eye guidelines. Single pixel size corresponds to 35 nm on the sample. The site $-L/2$ (in (b)) is where the first pulse arrived, the site $+L/2$ is location of the second (delayed) pulse.

in order to achieve the smallest energy of a recognizable modification. At such conditions the pulse duration is close to the measured spectral bandwidth-limited value of $\tau_p = 45 \pm 5$ fs in air. Once the chirp was optimized for the pump, part of the same pulse was used to generate a probe pulse for imaging. Precision of the time delay in pump-probe measurements was $\Delta t = \pm 10$ fs determined by precision of the optical delay line. Polarization of the pump pulses was linear; oriented horizontal in the image plane (Fig. 2).

3. Results and discussion

A new phenomenon observed after irradiation of two pump pulses was formation of side spots when spatial separation between the pulses was in the range of $\Delta x = 0.8 - 2$ μm. The side spots are transient or become permanent at higher pulse energies. First, we show that the experimentally observed densification - the side spots - separated by distance L of few micrometers (Fig. 2), are result of pressure waves generated by two pump pulses. Longitudinal and

#164236 - $15.00 USD Received 29 Mar 2012; revised 11 Apr 2012; accepted 17 Apr 2012; published 27 Apr 2012
(C) 2012 OSA

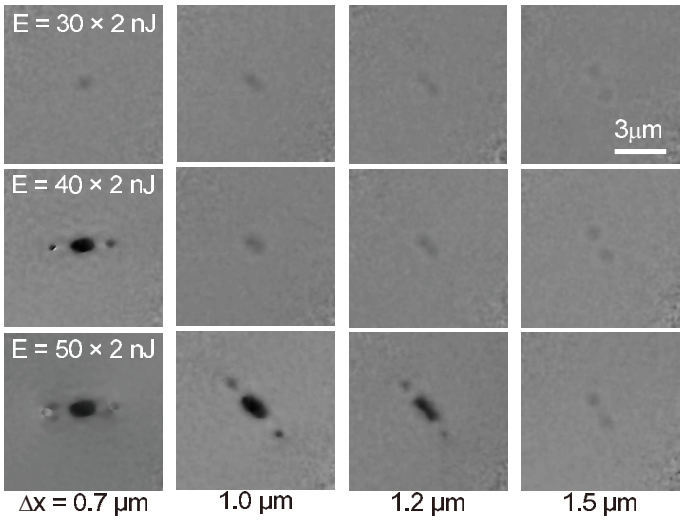

Fig. 4. Phase map vs separation between pulses, Δx, for $\Delta t = 0.2$ps and two pump energies $E_1 = E_2 = 30,\ 40,\ 50$ nJ. The site $-L/2$ (see, Fig. 3(a)) is where the first pulse arrived, the site $+L/2$ is location of the second (delayed) pulse.

transverse pressure waves in glass travels at velocities $v_{l,t}$, respectively, and their velocities are intra-related and defined as $v_l = \sqrt{B/\rho + \frac{4}{3}v_t^2}$ [37]. We set the origin point at the central point between two irradiation spots as $x = 0$ (Fig. 2) and we can assume that the stress wave is generated from an irradiation spot which has diameter $d \simeq 0.8\ \mu$m. We experimentally measure separation between the side spots, L, and diameter of the irradiation region d from Fig. 2. At the irradiation site, the delivered energy drives thermo elastic stress, launches a shock wave which dissipates to an ordinary pressure wave. For simplicity we assume sound wave propagation in further analysis as the shock waves are propagating at close to sound velocities even in the presence of strong breakdown [9, 38].

The faster longitudinal wave launched from one irradiation site will catch up the slower transverse wave traveling towards the location of the side spot; the two irradiation sites are separated by Δx. This condition when two waves launched with spatial separation of Δx at two different velocities catches up can be written as (for propagation along x-axis):

$$\frac{L/2 + \Delta x/2 + d/2}{v_l} = \frac{L/2 - \Delta x/2 + d/2}{v_t} \tag{1}$$

here we neglect time separation between two pulses, Δt, which is correct for separations smaller than 10 ps when sound travels only $v_l \times 10$ ps = 50 nm, which is below our spatial resolution. The term $d/2$ accounts for the location of the stress wave launch assumed to be at the rim of the focal spot.

With glass parameters given in Sec. 2 one would find solution of Eq. (1): $v_t = 3.2$ km/s and $v_l \simeq 5.4$ km/s (the v_l is the measured value in D263, Schott glass). This shows qualitatively that the observed side densified spots is a result of acoustic phenomenon when transverse and longitudinal excitation waves traverse each other. Apparently, when summation of the amplitudes of the two waves causes pressures in excess of material's elastic strength defined by the bulk modulus, a permanent densification at the side-spots can be induced as observed in experiments. Below that threshold, the densification is transient. Noteworthy, the transverse sound

#164236 - $15.00 USD Received 29 Mar 2012; revised 11 Apr 2012; accepted 17 Apr 2012; published 27 Apr 2012
(C) 2012 OSA

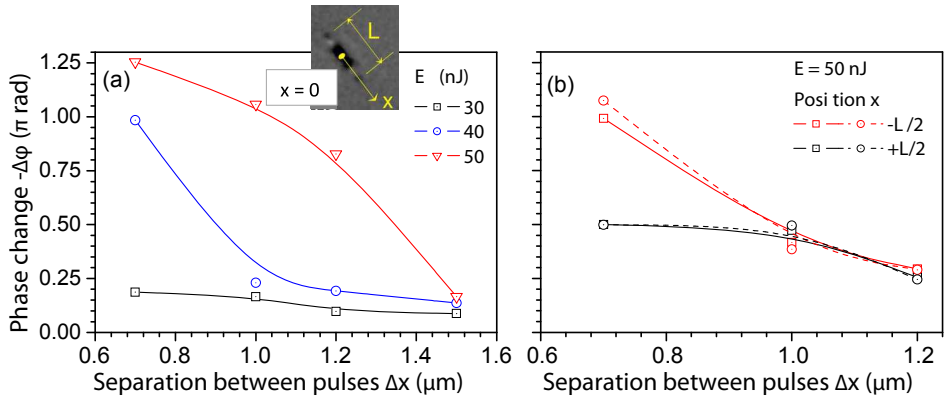

Fig. 5. (a) Phase at the location the middle point $x = 0$ vs separation between pulses, Δx, (see, Fig. 4) for $\Delta t = 0.2$ ps and pump energies of two pulses $E_1 = E_2 = 30;\ 40;\ 50$ nJ. (b) Phase at the locations $x = \pm L/2$ (side spots) vs separation between pulses, Δx, at pulse energy $E_p = 50$ nJ (two separate experiments). Lines are eye guidelines. The site $-L/2$ (see, Fig. 3(a)) is where the first pulse arrived, the site $+L/2$ is location of the second (delayed) pulse.

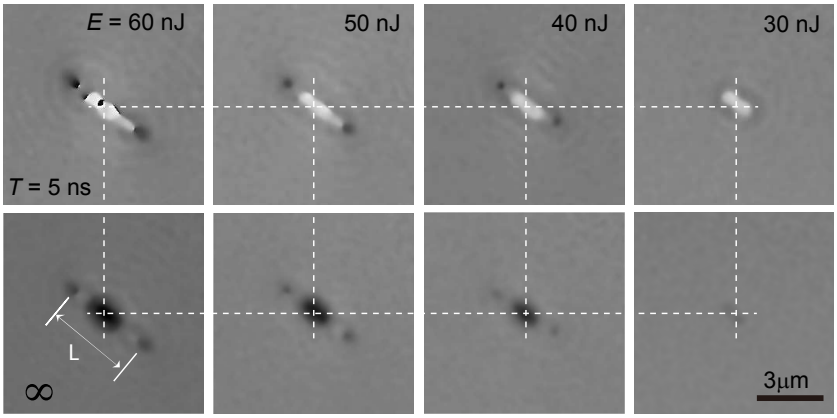

Fig. 6. Phase maps of photo-acoustically induced densification at different pulse energies of 30-60 nJ at $T = 5$ ns and after all relaxations; $\Delta t = 0.2$ ps, $\Delta x = 0.8$ μm. Separation between side spots, L, is increasing with pulse energy, E_p. Dashed lines are alignment eye guides. Phase spans from $-\pi$ to π. The site $-L/2$ (see, Fig. 3(a)) is where the first pulse arrived, the site $+L/2$ is location of the second (delayed) pulse.

wave does not induce mass density changes as it propagates, however, when it is added locally with longitudinal wave (which induces density changes) the overall effects reveals the densification. In the case of single pulse irradiation, side spots are not existent even at the cumulative two pulse pulse energies and above. Localization of the acoustically caused densification at the locations of side spots is $l_d \sim 0.4$ μm in cross section. Let us assume that the modification should be on the scale of the wavelength of the sound wave. For the sound speed of $v_l \simeq 5$ km/s this would correspond to the frequency $\nu = v_l/l_d \simeq 10$ GHz. This estimation shows that the high-frequency sound can be excited by the fast "instantaneous" heating and thermal stress

#164236 - $15.00 USD Received 29 Mar 2012; revised 11 Apr 2012; accepted 17 Apr 2012; published 27 Apr 2012
(C) 2012 OSA

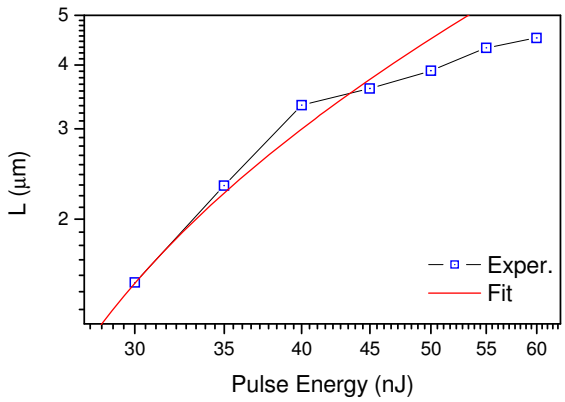

Fig. 7. Phase at the mid-point location $x = 0$ vs pulse energy: experiment (from Fig. 6) and linear fit by $\propto 0.15[\mu\text{m}](E - E_{th})$ with $E_{th} = 20$ nJ; ~ 0.15 μm is the most close distance two separate irradiation spots can be brought to. The pressure which is driving micro-explosion is proportional to the absorbed energy of the pulse of energy E. Note, both axes are logarithmic.

delivered by ultra-short femtosecond laser pulses [5].

Figure 3(a) shows how the phase is changing on the time separation, Δt, between two pulses at the middle point between two irradiation spots. The middle point at $x = 0$ is affected by the colliding elastic pressure waves traveling at the same velocity (at v_t and v_l) as well as by the heat diffusion from the irradiation locations. The later being the defining factor of the modification at high pump energy: first, the phase is positive (rarefied material) and becomes densified at the end of relaxation (darker regions in Fig. 4). As time separation becomes larger than 10 ps (see, Fig. 3), or approximately 50 nm in a sound travel length, the effect of the two wave collision and densification gradually disappears. At the side spots (Fig. 3(b)), phase changes are approximately twice smaller, $\Delta\phi_{max} \simeq -0.35\pi$ and are considerably more noisy. This is caused by a smaller size of phase change area since the phase is inferred from a single pixel which corresponds to a 35 nm cross section region on the sample. The stronger phases change was observed at the location closer to the spot which was irradiated first (at $x = -L/2$ in Fig. 3(b)); a similar time decay of the phase as that for the central point was observed as pulse separation become $\Delta t > 10$ ps. There was appearance of anti-phase changes at the two side spots Fig. 3(b), however they were not well resolved due to the phase noise.

Figure 4 shows phase maps and the extracted values are plotted separately for the middle and side points in Fig. 5 (for the pulses of different energy and at different separation L between the irradiation sites). As separation L increases, the side-spots gradually disappear (Figs. 4-5(b)). This is consistent with the pressure dissipation by $P \propto \frac{E}{r^3} \simeq P_s \left(\frac{r_s}{r}\right)^3$, where E is the absorbed energy driving shock, r is the radius, r_s is the effective radius of the pressure source, and P_s shock pressure amplitude at the source. The velocity of the shock wave scales as $v_{sh} \approx v_l \left(\frac{r_s}{r}\right)^{3/2}$ [39]. At small pulse energy of 30 nJ the phase depends on the separation, Δx linearly, while at higher energies nonlinearity becomes obvious (Fig. 5(a)). This could signify propagation of sound through regions of altered elastic or density, ρ, regions (note, $v_l = \sqrt{Y/\rho}$) or/and shock wave (longitudinal) transition to the sound wave which is not inducing phase changes larger than -0.2π. At the location of side spots (Fig. 5(b)), smaller phase changes were observed. There was a departure from linear dependence on pulse energy for the phase value as well as for the side spot separation, L, discussed next.

#164236 - $15.00 USD Received 29 Mar 2012; revised 11 Apr 2012; accepted 17 Apr 2012; published 27 Apr 2012
(C) 2012 OSA

The distance L between side densified regions depends on the pulse energy as shown in Fig. 6. As E_p increases, strong heating of irradiated regions is observed (bright regions in Fig. 6 at time moment $T = 5$ ns). Strong heating and glass melting reduces acoustic velocity. This explains why length L increases with pulse energy (Fig. 7). The pressure which drives micro-explosion scales with absorbed energy, however, when $E_p > 40$ nJ the proportionality fails. At those conditions, the pulse energy is already more than twice larger as required for the permanent modification to be recorded by a single pulse. The departure of $L \propto E^1$ indicates that validity of the Eq. (1) seizes as pulse energy is increased. However, the departure from linear scaling is gradual and the qualitative explanation of the observed side-spots phenomenon as being acoustically induced phenomenon is satisfactory.

It is interesting to see (Figs. 2, 4, and 6) that the central densification is not linearly proportional to the pulse energy as can be inferred from Fig. 5. A possible explanation is an absorption by free and trapped electrons which provides additional absorption channel. The free electrons generated by optical breakdown are recombining and thermalizing with ions on a few picosecond time scale. Recombination of electrons and holes proceeds via traps in glasses [40]. When separation of pulses in time becomes larger than 10 ps (an electronic excitation lifetime) we see strong decrease in the phase modification at the middle point between two laser irradiation spots (Fig. 3(a)).

Phase snap-shots show that at certain time moments phases singularities (see, Fig. 6) are developed around the irradiation locations and side spots. The singularities are recognizable as strongly laterally localized phase jumps over more than 2π. Such apparent phase changes are caused by large and spatially localized material density alterations. The phase singularity would change the wave front of the light wave propagating through such regions and an optical vortex would be generated in the transmission beam. Analysis of the light passed throughout the phase singularity can be carried out in the optical far-field by imaging and polariscopy [41]. Polarization analysis of the out going light provides a direct readout of the density changes at the singularity site and has capability of super-resolution as we demonstrated recently [42]. This method can be applied to characterize sub-wavelength modifications inside glasses and crystals.

4. Conclusions

We have demonstrated that propagating of acoustic excitations in glass can cause a permanent densification during direct laser writing by a pair of closely-spaced ultra-short laser pulses. Acoustic localization of energy within volumes of sub-micrometer cross sections takes place and is sensitive to the spatial and temporal separation of the writing pulses. Since direct fs-laser writing by few pulses and beam arrays is widely used in waveguide recording and micro-fabrication [43, 44], it is important to control this phenomenon. Similar effects are expected in other glass and crystalline materials [18, 22, 41, 45], where anisotropy can cause more complicated patterns of modification.

Acknowledgments

This work was supported by a Grant-in-Aid for Scientific Research (B) from the Ministry of Education, Culture, Sports, Science and Technology of Japan.

#164236 - $15.00 USD Received 29 Mar 2012; revised 11 Apr 2012; accepted 17 Apr 2012; published 27 Apr 2012
(C) 2012 OSA